Ionics
https://doi.org/10.1007/s11581-017-2323-3

ORIGINAL PAPER

Metal-organic framework-derived CoNi-embedded carbon nanocages as efficient electrocatalysts for oxygen evolution reaction

Zhiqiang Xie[1] · **Ying Wang**[1]

Received: 23 June 2017 / Revised: 23 October 2017 / Accepted: 24 October 2017

Abstract The major challenge of electrocatalytic water splitting for hydrogen production is the sluggish kinetics of oxygen evolution reaction (OER). Herein, we report a facile synthesis of CoNi alloy embedded carbon nanocages (CoNi-C) through one-step annealing treatment of bimetallic organic frameworks as the precursors for application as efficient and economical electrocatalysts for OER. As a result, the optimized CoNi-C-200 sample with a Co/Ni atomic ratio of 9:1 exhibits a lower overpotential of 408 mV at a current density of 10 mA cm^{-2} and a smaller Tafel slope of 83 mV dec^{-1} compared to as-prepared CoNi-C-100 (410 mV, 93 mV dec^{-1}), CoNi-C-400 (420 mV, 94 mV dec^{-1}), and Co-C (447 mV, 97 mV dec^{-1}). Moreover, it shows an excellent long-term stability during 5000 CV sweeps. Such improved performance can be attributed to the unique morphology and the synergistic effects of CoNi alloy nanoparticles and conductive carbon matrix in the composite.

Keywords CoNi alloy · Metal organic framework · Water splitting, electrocatalyst · Oxygen evolution reaction

Introduction

With ever-increasing energy demands and depletion of fossil fuels, extensive efforts have been devoted to exploring new sustainable and environment-friendly energy conversion and storage systems [1, 2]. Hydrogen has attracted wide attention as an efficient energy storage carrier, thanks to its abundant and sustainable nature [3]. In the present, electrolysis of water is considered as the most efficient ways to produce high-purity hydrogen at low cost [4, 5]. The splitting of water involves two half reactions [6, 7]. At the cathode, protons are reduced to hydrogen in the alkaline solution $2H_2O + 2e^- \rightarrow 2OH^- + H_2$ (hydrogen evolution reaction, HER). At the anode, four hydroxyl groups are oxidized to oxygen in alkaline solution $4OH^- \rightarrow O_2 + 2H_2O + 4e^-$ (oxygen evolution reaction, OER). The major challenge of water splitting is the sluggish kinetics of OER as compared to HER, which usually requires a large overpotential for multi-step transfer of four electrons [8]. Up to date, noble metal oxides such as ruthenium oxides (RuO_2) and iridium oxides (IrO_2) are efficient electrocatalysts for OER [9, 10]. Nevertheless, their large-scale applications are severely hindered by the high cost and scarcity of the noble metals. In addition, these noble metal oxides exhibit poor chemical stability in alkaline solution.

To overcome the aforementioned challenges, it is always desirable to explore new alternatives to replace noble metal oxides as low cost and efficient electrocatalysts for OER. To date, various noble metal-free electrocatalysts such as transition metal oxides [11], hydroxides [12], nitrides [13], sulfides [14], and phosphides [15] have been widely reported. Unfortunately, most of these materials are either limited by their low-electrical conductivities or poor-electrocatalytic activities, resulting in much higher overpotential at a current density of 10 mA cm^{-2} compared to RuO_2 (410 mV) [16]. Recently, transition metal alloys have attracted more and more interest, owing to their low cost and environmental benignity. So far, various transition metal alloys such as NiFe, NiCu, NiCe, and their composites have been explored for OER [17]. Despite much progress having been made in the

Electronic supplementary material The online version of this article (https://doi.org/10.1007/s11581-017-2323-3) contains supplementary material, which is available to authorized users.

✉ Ying Wang
ywang@lsu.edu

[1] Department of Mechanical and Industrial Engineering, Louisiana State University, Baton Rouge, LA 70803, USA

Published online: 15 November 2017

development of transition metal alloy-based catalyst for OER, the catalytic activity of OER is still not comparable to commercial noble metal oxide catalyst. Such limited performance is originated from the complex synthesis and much stricter requirement for the transition metal alloy-based catalysts such as chemical composition, particle size, and structural stability. Therefore, more efforts are highly needed to optimize the transition metal alloy-based catalysts for efficient OER.

Metal-organic frameworks (MOFs), built from metal ions/clusters as nodes and organic linkers as struts, have attracted more and more interest in recent years due to their high-surface area, large-pore volume, and diverse structures [18]. Inspired by these features, MOFs have been reported as new templates and precursors for synthesis of various hierarchical nanostructured materials such as porous carbons [19], metal oxides [20], metal/carbon composites [21], and metal oxides/carbon composites [22]. These MOF-derived nanostructures can offer many unique advantages: (i) the chemical composition can be easily tuned by designing MOFs combined with specific thermal treatment; (ii) MOF-derived nanostructures provide controlled porosity and huge surface area, which can effectively facilitate the access of electrolyte into the electrode and ensure large electrolyte/electrode contact area; (iii) the charge diffusion lengths can be largely shortened and thus facilitate the charge transfer for OER activity; (iv) the low cost and ease of synthesis allow MOF-derived nanostructures to be potentially scaled up for industrial applications. Up to now, transition metal alloy nanoparticles have emerged as new candidates for electrocatalyst for OER; however, the preparation of metal alloy/carbon nanostructures by using bimetallic MOFs as the single precursor has rarely been reported [23, 24]. Compared to other synthesis methods of alloy nanoparticles, one-step pyrolysis of bimetallic MOFs offers a facile route to prepare well-dispersed alloy nanoparticles embedded conductive carbon matrix without using any surfactants or toxic reducing agent. The chemical composition and particle size of alloy can also be optimized by simply varying the mixed metal ions ratio during the synthesis.

To combine the merits of transition metal alloy and MOF-derived nanostructures, we synthesized novel CoNi alloy embedded carbon nanocages (CoNi-C), through one-step pyrolysis of Co/Ni bimetallic metal organic framework (MOF) in argon atmosphere. Within such MOF-derived nanostructure, inner CoNi alloy nanoparticles can offer numerous active sites to efficiently catalyze the redox reactions, meanwhile the carbon nanocages serve as conductive network supporting the CoNi catalysts, which can effectively prevent CoNi nanoparticles from aggregation and reduce corrosion by alkaline electrolyte during long-term operation. As a result, CoNi-C-200 with a Co/Ni atomic ratio of 9:1 demonstrates obviously enhanced catalytic activity for OER in 1 M KOH aqueous solution compared with cobalt nanoparticles embedded nanocages (Co-C), showing a small overpotential of 408 mV for a current density of 10 mA cm^{-2} and a smaller overpotential of 366 mV after 5000 CV sweeps. To the best of our knowledge, this work is the first report on the application of MOF-derived transition metal alloys as efficient and robust catalysts for OER. We believe that the strategy presented here opens up a new route to development of versatile metal alloy/carbon nanocomposites for wide electrochemical applications, such as dye-sensitized solar cells, photocatalysts, and so forth.

Experimental

Preparation of Co-C and CoNi-C

The pure ZIF-67 powders were prepared according to previous reports with some modifications [25, 26]. In brief, 2 g cobalt nitrate hexahydrate and 3.06 g 2-methylimidazole were separately dissolved in 100 ml methanol, respectively. Afterwards, the two solutions were mixed under stirring for 10 min and aged for 24 h at room temperature. The resultant purple solid was collected from the solution by centrifugation at 4000 rpm for 10 min and then washed with methanol at least three times. After washing, the ZIF-67 powders were dried overnight at 80 °C. Afterwards, cobalt nanoparticles embedded within N-doped carbon nanocages (Co-C) were prepared by a facile calcination of ZIF-67 nanocrystals at 900 °C for 2 h in Ar atmosphere.

Similar to synthesis of ZIF-67, Co/Ni bimetallic MOFs were prepared by using 2 g cobalt nitrate hexahydrate, 3.06 g 2-methylimidazole, and different amounts of nickel nitrate hexahydrate (100, 200, 400 mg, respectively). Afterwards, Co/Ni-based MOFs were transformed to CoNi-C by a direct pyrolysis at 900 °C for 2 h in Ar atmosphere. For convenience, the as-prepared CoNi-C samples were labeled as CoNi-C-100, CoNi-C-200, and CoNi-C-400, respectively.

Characterizations

The crystalline structures of as-obtained products were identified by using X-ray diffraction (XRD) technique, and the data were recorded at a constant scanning rate of 2°/min on a Rigaku MiniFlex X-ray diffractometer (Cu Kα radiation). The microstructures and morphologies of samples were characterized by using scanning electron microscope (SEM) and high-resolution transmission electron microscope (HRTEM). The SEM imaging was carried out on a FEI Quanta 3D FEG FIB/SEM, which is equipped with energy-dispersive X-ray spectroscopy (EDS). TEM and HRTEM imaging was performed on a JEOL JEM-2010 microscope at 200 kV.

Electrochemical measurements

The electrochemical measurements were performed by using a CHI 760D electrochemical workstation (CH Instruments, Inc.) and a rotating disk electrode controller (AFMSRCE, Pine Instrument Co.). A platinum wire and Ag/AgCl electrode were used as counter electrode and reference electrode, respectively. The measured potentials vs. Ag/AgCl were converted to reversible hydrogen electrode (RHE).

To prepare catalyst film-coated glassy carbon working electrode, 8-mg powders were dispersed in 2 mL freshly prepared dispersion solution (Ethanol/Nafion = 100:1 (*V*/*V*)), following by sonication for 1 h. Afterwards, 10-μL fresh catalyst ink was deposited on a rotating disk electrode with geometric area of 0.196 cm^2 by a house-built spinning coating device under a gentle airflow.

The oxygen evolution reaction (OER) properties of the CoNi-C-100, CoNi-C-200 and CoNi-C-400, and Co-C catalysts were studied using linear sweep voltammetry (LSV). The potential was swept at a scan rate of 5 mV s^{-1} and an electrode rotation rate of 1600 rpm in N_2-saturated 1 M KOH aqueous solution. The electrochemical impedance spectroscopy (EIS) measurements were carried out in the frequency range from 10^5 to 0.01 Hz using an electrochemical workstation (CHI 6504C). To study the electrochemical stability of as-prepared electrocatalysts, the cyclic voltammetry (CV) was carried out at a scan rate of 100 mV s^{-1} for up to 5000 cycles.

Results and discussion

The overall synthesis of MOF-derived CoNi-C nanostructures involves two steps. In the first step, the Co/Ni bimetallic metal organic frameworks (MOFs) are synthesized using various ratio of Co^{2+}/Ni^{2+} and 2-methylimidazole at room temperature. During the following pyrolysis process at 900 °C for 2 h, Co^{2+} and Ni^{2+} are simultaneously reduced into metallic Co and Ni by the resultant carbon from the decomposition of organic linkers at high temperature, and meanwhile, metallic Co and Ni undergo the alloying reaction process to form CoNi alloy nanoparticles, which can subsequently function as catalyst to promote the formation of onion-like carbon around them.

To identify the crystalline structures and phases of the MOF-derived CoNi-C samples, the powder X-ray diffraction (XRD) measurements are first performed. The XRD results show that all the CoNi-C samples are composed of graphitic carbon and face-centered cubic (fcc) CoNi alloy (Fig. 1a). It is clearly observed that the strongest (111) reflection peak positions of all samples lie between the peak position of pure Co (JCPDS# 15-0806) and pure Ni (JCPDS# 04-0850) (Fig. 1b), which is well consistent with previously reported CoNi alloys [27, 28]. The main (111) peaks of CoNi-C samples obviously shift to higher angles with the increase of Ni^{2+} amounts during the synthesis, further confirming the formation of CoNi alloys. No other impurities or phases are observed, implying a complete transformation of Ni^{2+} incorporated ZIF-67 to CoNi-C. In addition, the sharp peaks in the XRD spectra of the CoNi alloy indicate that the samples are highly crystalline.

SEM images (Fig. S1) show that ZIF-67 samples are composed of polyhedron-like particles with smooth surfaces. After one-step pyrolysis process in inert gas atmosphere, the low-magnification SEM images in Fig. 2a and c show that the as-synthesized CoNi@-C-100 and CoNi-C-200 samples consist of polyhedron-like carbon nanocages (200 ~ 500 nm) with CoNi alloy nanoparticles well-embedded. By comparison of high-magnification SEM images in Fig. 2b and d, it is

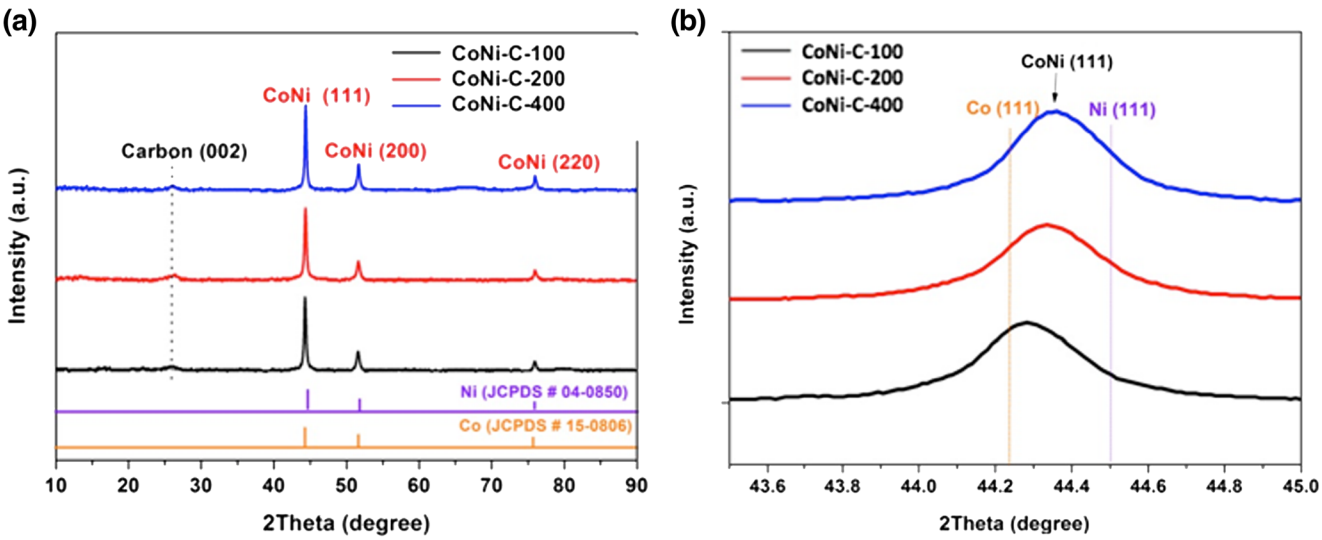

Fig. 1 **a** XRD patterns and **b** selected enlarged portion of CoNi-C-100, CoNi-C-200, and CoNi-C-400 samples in comparison with standard XRD peaks of pure Co and Ni

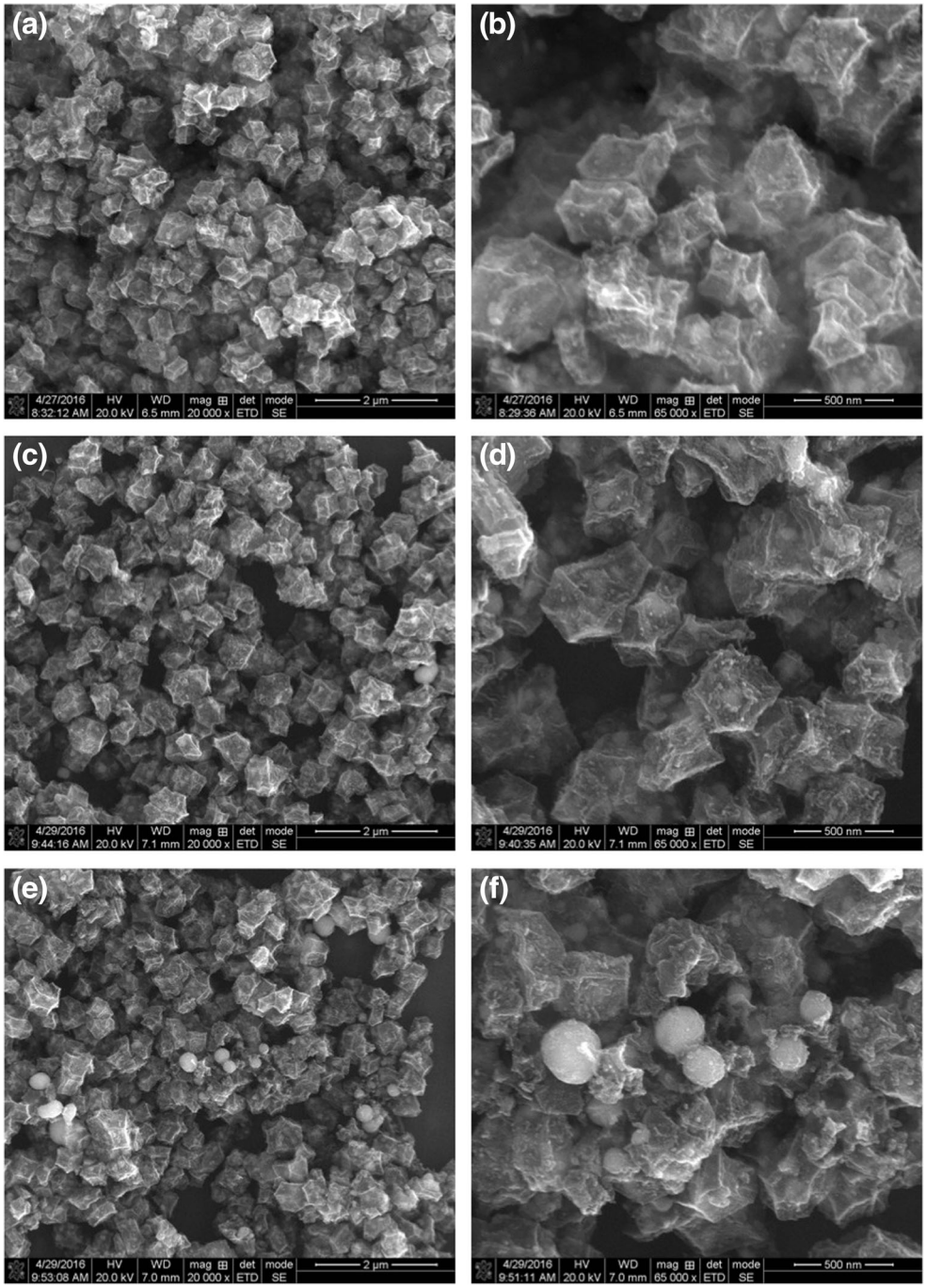

Fig. 2 SEM images of **a**, **b** CoNi-C-100, **c**, **d** CoNi-C-200, and **e**, **f** CoNi-C-400

observed that larger particles are embedded within the carbon nanocages in the CoNi-C-200 sample than CoNi-C-100. On the contrary, some of the carbon nanocages in CoNi-C-400 sample are broken and one can notice that relatively larger CoNi alloy particles are located outside the carbon nanocages (Fig. 2e–f). This observation indicates that the Ni amount plays a crucial role in control of the particle size of CoNi alloy.

Experiments presented further in the work show that the catalyst based on the CoNi-C-200 demonstrates the highest catalytic activity for OER, and therefore, we perform detailed transmission electron microscopy (TEM) and high-resolution (HR) TEM characterizations for better visualization of its nanostructure, as displayed in Fig. 3a–d. It can be clearly observed that CoNi alloy nanoparticles with the size of 20 ~ 100 nm (dark dots) are well embedded in carbon nanocages (gray framework) in CoNi-C-200 sample. Interestingly, one can observe that CoNi nanoparticles are encapsulated by onion-like carbon (marked by blue arrows in Fig. 3d). As we can see from the inset in Fig. 3d, the distinct lattice fringe with the measured d-

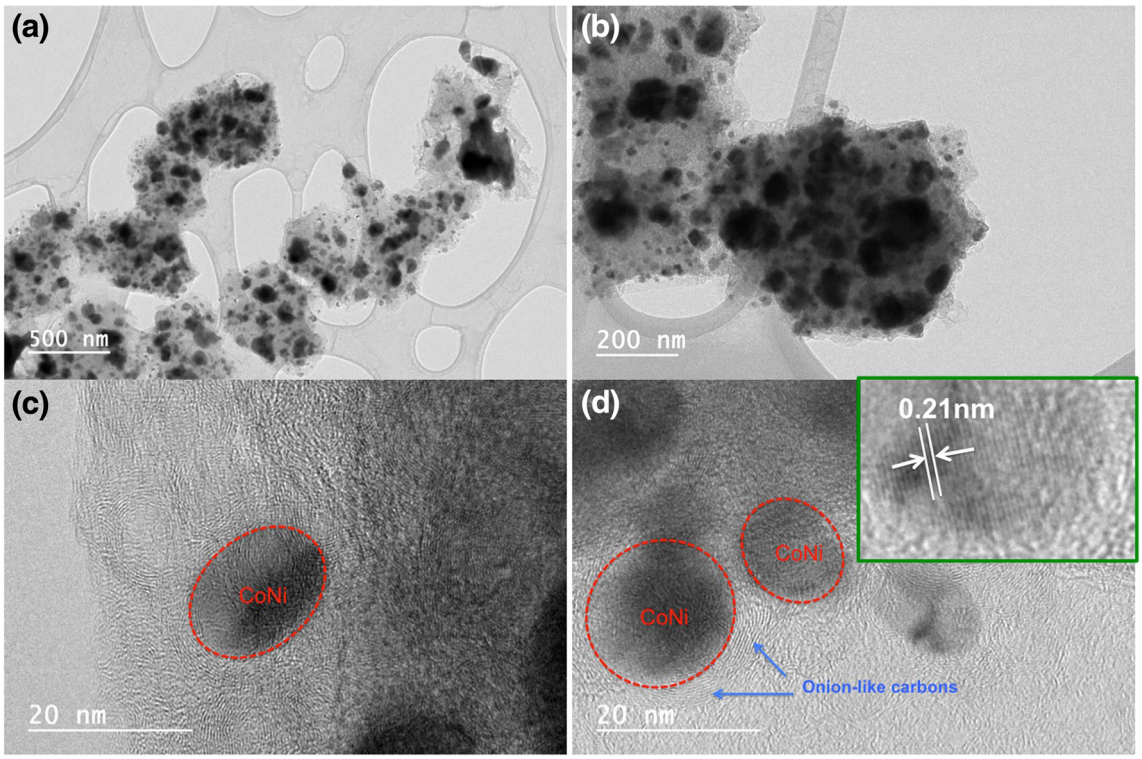

Fig. 3 **a**, **b** TEM images and **c**, **d** HRTEM images of CoNi-C-200 (optimal sample)

spacing of 0.21 nm can be assigned to the (111) plane of CoNi alloy, which further confirms successful formation of MOF-derived CoNi alloy through a facile one-step pyrolysis process in inert gas atmosphere. Thus, the SEM and TEM observations above indicate that we have successfully obtained the CoNi-C sample with a unique nanostructure, whereas CoNi alloy nanoparticles are well encapsulated into the onion-like carbon, meanwhile they are completely embedded into carbon nanocages.

The corresponding energy-dispersive X-ray (EDS) mapping results further confirm the coexistence of C, Co, and Ni elements within the sample, and both Co and Ni elements show homogeneous distribution for the inner nanoparticles within the carbon nanocages (Fig. S2), confirming the CoNi alloy phase which are well consistent with previous XRD and TEM results. It is also worth noting that chemical composition of the as-prepared CoNi alloy in our work can be easily tuned by varying the atomic ratio of cobalt and nickel ions during the

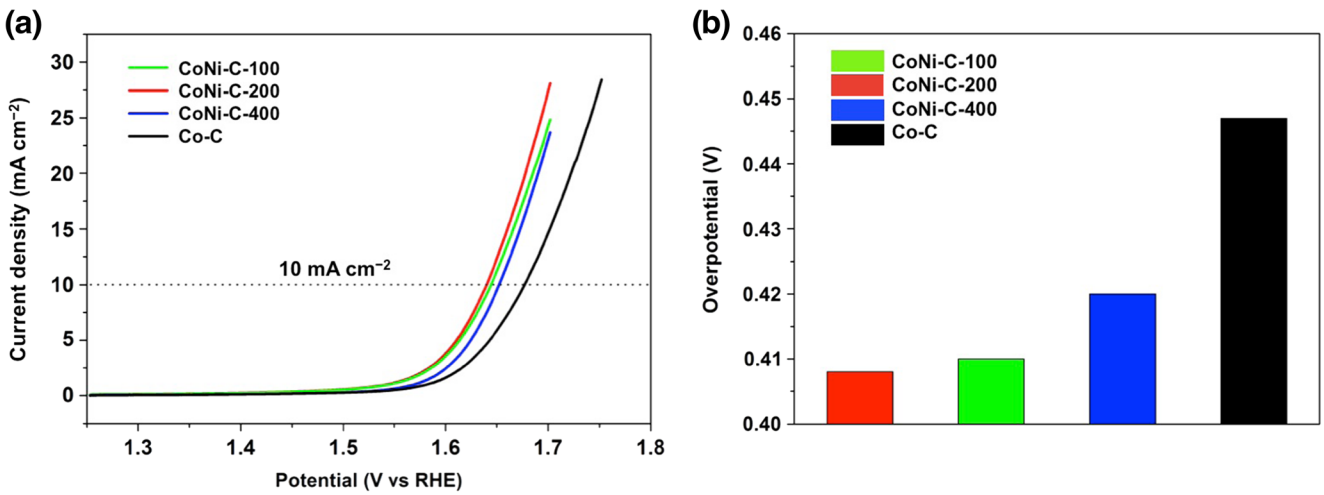

Fig. 4 **a** Comparison of OER polarization curves of CoNi-C-100, CoNi-C-200, CoNi-C-400, and Co-C, measured in 1 M KOH aqueous solutions at a scan rate of 5 mV s^{-1}. **b** The overpotentials needed to reach a current density of 10 mA cm^{-2} for the above four catalysts

synthesis of Ni^{2+}-incorporated ZIF-67 nanocrystals. The atomic ratio of Co/Ni in the optimal sample CoNi-C-200 is found to be 9:1 through EDS mapping results, indicating a certain amount of Ni ions can be encapsulated within ZIF-67 nanocrystals during the synthesis process in methanol at room temperature. Thanks to such a unique hierarchical nanostructure composed of CoNi embedded carbon nanocages, the as-prepared CoNi-C composites are explored as catalysts for OER for the first time.

The catalytic activities of CoNi-C-100, CoNi-C-200, CoNi-C-400, and Co-C for OER are measured using a typical three-electrode system in 1 M KOH aqueous solutions. The potentials reported in this paper are all versus reversible hydrogen electrode (RHE). Figure 4a shows the linear sweep voltammetry (LSV) curves of all the electrodes at a scan rate of 5 mV s^{-1}. The polarization curve from the CoNi-C-200 catalyst exhibits the smallest onset potential of ~ 1.638 V and highest current density. As shown in Fig. 4b, the overpotential of CoNi-C-200 catalyst is 408 mV at the current density of 10 mA cm^{-2}, which is slightly lower than CoNi-C-100 (410 mV) and CoNi-C-400 (420 mV). These results indicate that the intrinsic OER activities for these three CoNi-based catalysts are similar. The difference in OER current densities could be attributed to the different number of active sites and surface area needed for electron transfer and ion transport in the catalysts. The ion transport refers to the OH^- adsorption and transfer to the active sites in the electrocatalysts. In contrast, the Co-C catalyst has much higher overpotential of 447 mV, showing the worst catalytic activity for OER. Therefore, it can be concluded that the CoNi alloy-based catalysts exhibit significantly enhanced OER activity compared to Co-C catalyst. This result can be attributed to the synergistic effects of Co and Ni in the alloy. Specifically, the incorporation of a secondary transition metal Ni results in the OH^- adsorption energies alteration via tuning the lattice and bond length of the crystal, favoring the OER catalytic activities [29, 30]. Comparing our optimal sample with other previously reported electrocatalysts for OER, it is found that CoNi-C-200 demonstrates a lower overpotential than IrO_2 (450 mV) [31], $Mn_3O_4/CoSe_2$ (450 mV) [32], and N-graphene/CNT (420 mV) [33]. In addition, its electrocatalytic performance is even comparable to commercial noble Ir/C (390 mV) [34]. Instead of using expensive noble metal or metal oxides as electrocatalysts, our work shows that the CoNi-C-200 holds great potential as an efficient and economical electrocatalyst for OER.

To better understand the OER electrochemical kinetics, we fit the polarization curves to the Tafel equation $\eta = b^*\log(j)$, where η is the overpotential, b is the Tafel slope, and j is the current density [35, 36]. A smaller Tafel slope value represents a smaller increase in overpotential, corresponding to a more efficient OER activity [37, 38]. The Tafel slope plots, along with the slope values, are shown in Fig. 5. The Tafel slopes of

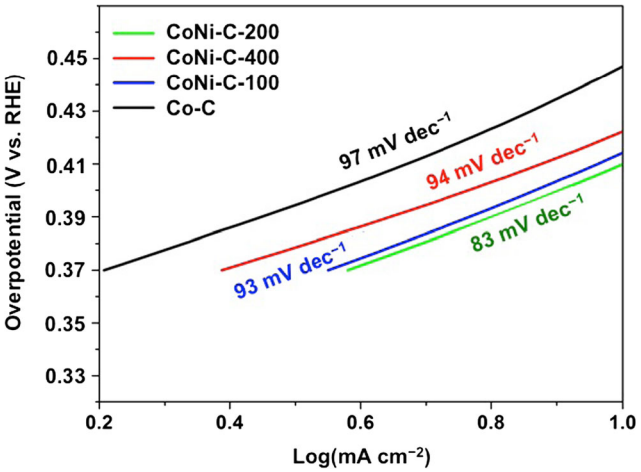

Fig. 5 **a** Tafel plots of CoNi-C-100, CoNi-C-200, CoNi-C-400, and Co-C, measured in 1 M KOH aqueous solutions

CoNi-C-100, CoNi-C-200, CoNi-C-400, and Co-C are 93, 83, 94, and 97 mV dec^{-1}, respectively. The CoNi-C-200 catalyst displays the smallest Tafel slope in 1 M KOH aqueous solutions, indicating the best catalytic activity for OER.

In addition to high-catalytic activity, durability is another critical parameter that determines the practical application of catalysts for OER. Thus, in this study, we perform an accelerated degradation test for evaluation of OER stability. As shown in Fig. 6, the polarization curves of CoNi-C-200 (the optimal sample) are recorded after 0, 100, 200, 300, 400, 500, 1000, and 5000 CV sweeps at a scan rate of 100 mV s^{-1}. It is interesting to notice a current density increase and reduction of overpotential during the initial 300 CV sweeps. The polarization curves of CoNi-C-200 show a negligible change from 300 to 5000 CV sweeps, indicating its superior long-term stability as a robust catalyst for OER. It is worth mentioning that CoNi-C-200 exhibits a smaller overpotential of 366 mV after 5000 CV sweeps.

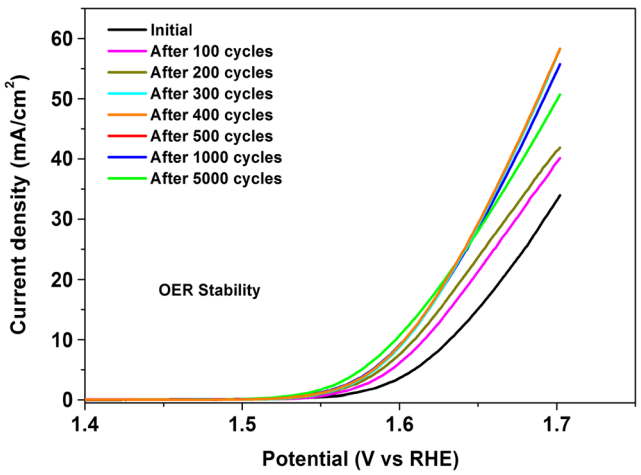

Fig. 6 OER stability test (5000 CV sweeps) of CoNi-C-200 (the optimal sample) in 1 M KOH aqueous solution at a scan rate of 100 mV s^{-1}

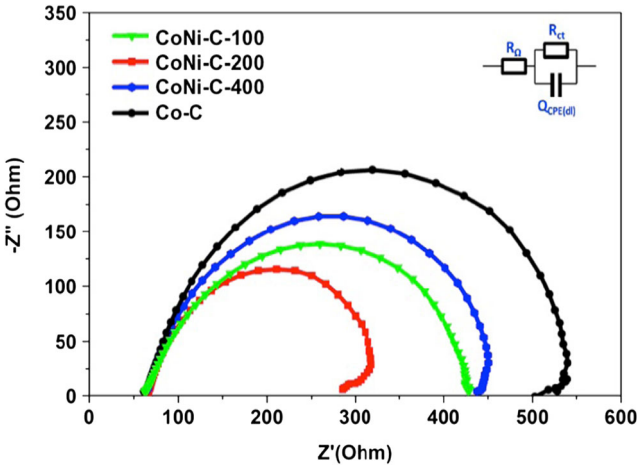

Fig. 7 Nyquist plots of CoNi-C-100, CoNi-C-200, CoNi-C-400, and Co-C electrodes tested at E = 1.638 V

Electrochemical impedance spectroscopy (EIS) measurements are conducted to provide further insight into the kinetics of catalytic reactions of as-prepared catalysts. Figure 7 displays typical Nyquist plots of CoNi-C-100, CoNi-C-200, CoNi-C-400, and Co-C electrodes when tested at E = 1.638 V in the 1 M KOH electrolyte. As we can see that all Nyquist plots are composed of depressed semicircles corresponding to the charge-transfer process for the OER. The Nyquist plots are fitted and can be represented by one capacitive loop, cell resistance (R_{Ω}) and the charge-transfer resistance (R_{ct}) for the OER. The depressed semicircle corresponds to the R_{ct}. According to previous reports [35, 36], smaller R_{ct} usually indicates higher catalytic activity for OER. As we can see from Fig. 6 that the four catalysts exhibit similar R_{Ω}, however, it is clearly observed that CoNi-C-200 shows a smaller semicircle than other catalysts, indicating the best catalytic activity among all the catalysts. These results are in good accordance with the LSV observations.

All the electrochemical measurements above indicate that CoNi-C catalysts exhibit high-catalytic activity and good durability for OER. For practical application in a real industrial water-splitting cell, the cost of electrocatalysts is another crucial factor that has to be taken into account. Unlike the scarcity and high cost of noble metal or their metal oxides as commercial OER electrocatalysts, the elements of CoNi-C catalysts are earth abundant and less expensive. Thus, the CoNi-C catalysts can be produced at low cost on a large scale. Furthermore, the whole synthesis procedure of CoNi-C catalysts is facile and economical due to the use of cheap precursors and simple one-step annealing treatment, which offers great potential in large-scale production of catalysts for water-splitting application. Considering both excellent OER performance and low cost of catalysts, we believe the CoNi-C catalysts hold great promise in water-splitting applications. In the future, we plan to fabricate a massive electrode by coating the as-prepared catalysts onto a large-sized substrate and investigate its OER performance for a real industrial water-splitting cell.

Conclusions

In summary, for the first time, we report a facile synthesis of CoNi-embedded carbon nanocages by direct pyrolysis of bimetallic metal organic frameworks in inert gas atmosphere and study their electrocatalytic performance in OER. It is found that CoNi-C-200 shows a small overpotential of 408 mV at a current density of 10 mA cm^{-2} and a small Tafel slope of 83 mV dec^{-1}, demonstrating the best catalytic activity for OER compared to CoNi-C-100, CoNi-C-400, and Co-C catalysts. In addition, CoNi-C-200 exhibits a smaller overpotential of 366 mV after 5000 CV sweeps, indicating a superior long-term stability. The enhancement in catalytic activity and long-term electrochemical stability can be attributed to the unique morphology and the synergistic effects of CoNi alloy and carbon component in the composite. Considering the facile synthesis of catalysts and their excellent catalytic activities in alkaline medium, the CoNi-C-200 shows great potential as an economic catalyst for OER applications. In addition, this work may open up a new route for further study of various metal organic frameworks as templates in design and development of low cost and efficient catalysts for OER. Due to its unique structure and superior properties, the as-prepared CoNi-C-200 may also find wide applications in other fields such as dye-sensitized solar cells, photocatalysts, and so forth.

Acknowledgements The authors would like to acknowledge the Research Enhancement Awards (REA) sponsored by LaSPACE and LSU Economic Development Assistantship for financial support. We also would like to acknowledge Changlin Zhang in Prof. Zhenmeng Peng's research group in Department of Chemical and Bimolecular Engineering at University of Akron for their contribution to this work. We want to thank the shared instrumentation facility (SIF) at Louisiana State University (LSU) for materials characterizations.

Compliance with ethical standards

Conflicts of interest The authors declare that they have no conflicts of interest.

References

1. Xu WW, Zhao KN, Zhang L, Xie ZQ, Cai ZY, Wang Y (2016) SnS_2@graphene nanosheet arrays grown on carbon cloth as free-standing binder-free flexible anodes for advanced sodium batteries. J Alloys Compd 654:357–362
2. Xie ZQ, WW X, Cui XD, Wang Y (2017) Recent progress in metal-organic frameworks and their derived nanostructures for energy and environmental applications. ChemSusChem. https://doi.org/10.1002/cssc.201601855

3. Mao S, Wen Z, Huang T, Hou Y, Chen J (2014) High-performance bi-functional electrocatalysts of 3D crumpled graphene–cobalt oxide nanohybrids for oxygen reduction and evolution reactions. Energy Environ Science 7:609–616
4. Flis-Kabulska I, Flis J, Sun Y, Zakroczymski T (2015) Hydrogen evolution on plasma carburised nickel and effect of iron deposition from the electrolyte in alkaline water electrolysis. Electrochim Acta 167:61–68
5. Sato J, Saito N, Yamada Y, Maeda K, Takata T, Kondo JN, Hara M, Kobayashi H, Domen K, Inoue Y (2005) RuO_2-loaded β-Ge_3N_4 as a non-oxide photocatalyst for overall water splitting. J Am Chem Soc 127:4150–4151
6. Bian W, Yang Z, Strasser P, Yang R (2014) A $CoFe_2O_4$/graphene nanohybrid as an efficient bi-functional electrocatalyst for oxygen reduction and oxygen evolution. J Power Sources 250:196–203
7. Su YZ, Xu QZ, Zhong QS, Shi ST, Zhang CJ, Xu CW (2014) $NiCo_2O_4$/C prepared by one-step intermittent microwave heating method for oxygen evolution reaction in splitter. J. Alloys Compd 617:115–119
8. Xiao M, Tian Y, Yan Y, Feng K, Miao Y (2015) Electrodeposition of $Ni(OH)_2$/NiOOH in the presence of urea for the improved oxygen evolution. Electrochim Acta 164:196–202
9. Lee Y, Suntivich J, May KJ, Perry EE, Shao-Horn Y (2012) Synthesis and activities of rutile IrO_2 and RuO_2 nanoparticles for oxygen evolution in acid and alkaline solutions. J Phys Chem Lett 3:399–404
10. Qiu Y, Xin L, Li W (2014) Electrocatalytic oxygen evolution over supported small amorphous Ni-Fe nanoparticles in alkaline electrolyte. Langmuir 30:7893–7901
11. Liang YY, Li YG, Wang HL, Zhou JG, Wang J, Regier T, Dai HJ (2011) Co_3O_4 nanocrystals on graphene as a synergistic catalyst for oxygen reduction reaction. Nat Mater 10:780–786
12. Song F, Hu X (2014) Ultrathin cobalt-manganese layered double hydroxide is an efficient oxygen evolution catalyst. J Am Chem Soc 136:16481–16484
13. Tian JQ, Liu Q, Asiri AM, Alamry KA, Sun XP (2014) Ultrathin graphitic C_3N_4 nanosheets/graphene composites: efficient organic electrocatalyst for oxygen evolution reaction. ChemSusChem 7: 2125–2130
14. Liu Q, Jin JT, Zhang JY (2013) $NiCo_2S_4$@graphene as a bifunctional electrocatalyst for oxygen reduction and evolution reactions. ACS Appl Mater Interfaces 5:5002–5008
15. Xiong DH, Wang XG, Li W, Liu LF (2016) Facile synthesis of iron phosphide nanorods for efficient and durable electrochemical oxygen evolution. Chem Commun 52:8711–8714
16. Gao MR, Gao Q, YF X, Zheng YR, Jiang J, SH Y (2014) Nitrogen-doped graphene supported $CoSe_2$ nanobelt composite catalyst for efficient water oxidation. ACS Nano 8:3970–3978
17. Chen S, Thind SS, Chen AC (2016) Nanostructured materials for water splitting-state of the art and future needs: a mini-review. Electrochem Commun 63:10–17
18. Cui XD, Xie ZQ, Wang Y (2016) Novel CoS_2 embedded carbon nanocages by direct sulfurizing metal–organic frameworks for dye-sensitized solar cells. Nano 8:11984–11992
19. Xie ZQ, He ZY, Feng XH, WW X, Cui XD, Zhang JH, Yan C, Carreon MA, Liu Z, Wang Y (2016) Hierarchical sandwich-like structure of ultrafine N-rich porous carbon nanospheres grown on graphene sheets as superior lithium-ion battery anodes. ACS Appl Mater Interfaces 8:10324–10333
20. Cho W, Lee YH, Lee HJ, Oh M (2009) Systematic transformation of coordination polymer particles to hollow and non-hollow In_2O_3 with pre-defined morphology. Chem Commun 31:4756–4758
21. Xia W, Zou RQ, An L, Xia DG, Guo SJ (2015) A metal–organic framework route to in situ encapsulation of Co@Co_3O_4@C core@bishell nanoparticles into a highly ordered porous carbon matrix for oxygen reduction. Energy Environ Science 8:568–576
22. Hou Y, Li JY, Wen ZH, Cui SM, Yuan C, Chen JH (2015) Co_3O_4 nanoparticles embedded in nitrogen-doped porous carbon dodecahedrons with enhanced electrochemical properties for lithium storage and water splitting. Nano Energy 12:1–8
23. Yu LT, Liu J, Xu XJ, Zhang LG, Hu RZ, Liu JW, Yang LC, Zhu M (2016) Metal-organic framework-derived NiSb alloy embedded in carbon hollow spheres as superior lithium-ion battery anodes. ACS Appl Mater Interfaces. https://doi.org/10.1021/acsami.6b14233
24. Li XN, Rykov AI, Zhang B, Zhang YJ, Wang JH (2016) Graphene encapsulated Fe_xCo_y nanocages derived from metal-organic frameworks as efficient activators for peroxymonosulfate. Catal Sci Technol 6:7486–7494
25. Banerjee R, Phan A, Wang B, Knobler C, Furukawa H, O'keeffe M, Yaghi OM (2008) High-throughput synthesis of zeolitic imidazolate frameworks and application to CO_2 capture. Science 319:939–943
26. WW X, Xie ZQ, Wang Z, Dietrich G, Wang Y (2016) Interwoven heterostructural Co_3O_4–carbon@FeOOH hollow polyhedrons with improved electrochemical performance. J Mater Chem A 4:19011–19018
27. MJ H, Lin B, SH Y (2008) Magnetic field-induced solvothermal synthesis of one-dimensional assemblies of Ni-Co alloy microstructures. Nano Res 1:303–313
28. Hu MJ, Lu Y, Zhang S, Guo SR, Lin B, Zheng M, Yu SH (2008) High yield synthesis of bracelet-like hydrophilic Ni-Co magnetic alloy flux-closure nanorings. J Am Chem Soc 130:11606–11607
29. Saha S, Ganguli AK (2017) FeCoNi alloy as noble metal-free electrocatalyst for oxygen evolution reaction (OER). Chemist Select 2:1630–1636
30. Wang JH, Cui W, Liu Q, Xing ZC, Asiri AM, Sun XP (2016) Recent progress in cobalt-based heterogeneous catalysts for electrochemical water splitting. Adv Mater 28:215–230
31. Zheng YR, Gao MR, Gao Q, Li HH, Xu J, ZY W, SH Y (2015) An efficient CeO_2/$CoSe_2$ nanobelt composite for electrochemical water oxidation. Small 11:182–188
32. Gao MR, Xu YF, Jiang J, Zheng YR, Yu SH (2012) Water oxidation electrocatalyzed by an efficient Mn_3O_4/$CoSe_2$ nanocomposite. J Am Chem Soc 134:2930–2933
33. Wen ZH, Ci SQ, Hou Y, Chen JH (2014) Facile one-pot, one-step synthesis of a carbon nanoarchitecture for an advanced multifunctonal electrocatalyst. Angew Chem Int Ed 53:6496–6500
34. Hou Y, Cui SM, Wen ZH, Guo XR, Feng XL, Chen JH (2015) Strongly coupled 3D hybrids of N-doped porous carbon nanosheet/CoNi alloy-encapsulated carbon nanotubes for enhanced electrocatalysis. Small 11:5940–5948
35. Zhang CL, Wang BW, Shen XC, Liu JW, Kong XK, Chuang SC, Yang D, Dong AG, Peng ZM (2016) A nitrogen-doped ordered mesoporous carbon/graphene framework as bifunctional electrocatalyst for oxygen reduction and evolution reactions. Nano Energy 30:503–510
36. Han GQ, Liu YR, Hu WH, Dong B, Li X, Shang X, Chai YM, Liu YQ, Liu CG (2016) Crystallographic structure and morphology transformation of MnO_2 nanorods as efficient electrocatalysts for oxygen evolution reaction. J Electrochem Soc 163:H67–H73
37. Li M, Liu TT, Fan LQ, Bo XJ, Guo LP (2016) Three-dimensional hierarchical meso/macroporous Fe/Co-nitrogendoped carbon encapsulated FeCo alloy nanoparticles prepared without any template or surfactant: high-performance bifunctional oxygen electrodes. J Alloys Compd 686:467–478
38. Yoon S, Yun JY, Lim JH, Yoo BY (2017) Enhanced electrocatalytic properties of electrodeposited amorphous cobalt-nickel hydroxide nanosheets on nickel foam by the formation of nickel nanocones for the oxygen evolution reaction. J Alloys Compd 693:964–999